Int J Adv Manuf Technol (2017) 89:2821–2836
DOI 10.1007/s00170-016-9618-9

ORIGINAL ARTICLE

Simulation of forced vibration in milling process considering gyroscopic moment and rotary inertia

Mohammad Mahdi Jalili[1] · **Jamal Hesabi**[1] · **Mohammad Mahdi Abootorabi**[1]

Received: 31 July 2016 / Accepted: 13 October 2016 / Published online: 11 November 2016

Abstract Prevention of resonance in vibration of cutting tool is essential for achieving high quality and efficiency of the milling process. The resonance causes the cutting tool to oscillate with great amplitude and increases cutting tool wear and production costs. Using a 3-D nonlinear dynamic model of the milling process including both structural and cutting force nonlinearities, gyroscopic moment, and rotary inertia, different types of resonances in milling process are investigated in this article. The cutting tool is modeled as a rotating clamped-free beam which is excited by cutting forces. Using the method of multiple scales, frequency response function of the system in primary and super harmonic resonances is obtained. Using this model, the influences of axial depth of cut, cutting tool diameter, cutting tool length, and the number of cutter teeth on the frequency response of the tool tip vibrations are studied. The results showed that increase of axial depth of cut increases the steady state vibration response of the tool tip in all resonance cases.

Keywords Milling process · Primary resonance · Super harmonic resonance · Nonlinear model · Method of multiple scales

✉ Mohammad Mahdi Jalili
jalili@yazd.ac.ir

Jamal Hesabi
jamal.hesabi@yahoo.com

Mohammad Mahdi Abootorabi
abootorabi@yazd.ac.ir

[1] Department of Mechanical Engineering, Yazd University, P.O. Box 89195-741, Yazd, Iran

Abbreviations

A	cross-sectional area
E	Young's modulus
F_r	feed (radial) cutting force
F_t	tangential cutting force
G	shear modulus
I	diametrical mass moment of inertia
J	polar mass moment of inertia
K_{tc}	the cutting coefficient contributed by the shearing in tangential direction
K_{te}	the cutting coefficient contributed by the edge action in tangential direction
K_{rc}	the cutting coefficient contributed by the shearing in radial direction
K_{re}	the cutting coefficient contributed by the edge action in radial direction
L_v, L_w	components of generalized nonconservative forces in y and z directions
N	number of teeth cutting tool
R	tool radius
U	strain energy
X, Y, Z	inertial coordinate system
A	depth of cut
$b(U), b(T)$	Strain and kinetic energy boundary terms
c_f	feed per tooth per revolution
D	tool diameter
v, w	transverse displacement
$\vec{i}, \vec{j}, \vec{k}$	unit vectors associated with deformed beam coordinate system
L	length of tool
ρ	density of the tool material
φ	elastic torsion about the elastic axis
ϕ_1, ϕ_2, ϕ_3	Euler angles
τ	period of tool revolution
Ω	tool rotational speed

$\sigma_{xx}, \sigma_{xy}, \sigma_{xz}$	engineering stress components
$\varepsilon_{xx}, \varepsilon_{xy}, \varepsilon_{xz}$	engineering strain components
$(\,)_{tran}$	related to translation
$(\,)_{rot}$	related to rotation
$\delta(\,)$	variation of $(\,)$
$(\,)'$	$\partial/\partial x$
$\dot{(\,)}$	$\partial/\partial t$
$\vec{(\,)}$	denotes vector

1 Introduction

Milling is one of the main machining processes used extensively in industrial productions. The generation of complex shapes with high quality for various types of materials is the main advantage of the milling process in contrast to other machining processes. Prediction and prevention of chatter vibration and resonance are essential for achieving high quality and efficiency of this process. Occurrence of chatter and vibration resonance during milling may cause damage to tool, spindle bearing, or the workpiece or may result in poor dimensional accuracy and surface finish of the workpiece.

In recent decades, an extensive number of efforts have been done to understand chatter in milling process. In the early works, modeling and analysis of the complex geometry and relative motion of workpiece/tool in milling process was carried out. Material nonlinearity, structural nonlinearities, nonlinearities due to tool/workpiece geometry, and high order nonlinear terms in the cutting force are the major sources of nonlinearity included in cutting models. Several mathematical methods, such as the bifurcation theory, perturbation analysis, phase portraits, and Poincare section, are developed and used for nonlinear dynamic analysis. Many researches have been carried out for chatter prediction, detection, suppression, and elimination. For example, Balachandran and Zhao developed multiple degrees of freedom model to identify the instabilities that may occur due to regenerative and/or loss of contact effects [1]. They predicted instabilities and explored motions beyond the instability or bifurcation locations. Mann et al. used a 2-DOF linear tool model to analyze the effects of asymmetric structural modes and the nonlinear regeneration in a discontinuous cutting force model of milling process [2]. Their investigations show hysteresis in bifurcation diagrams and the presence of coexisting periodic and quasi-periodic attractors. Vela-Martinez et al. developed a weak nonlinear model in both structural stiffness and regenerative terms to demonstrate the self-excited vibrations in machining [3]. They derived an approximate solution for this problem using the method of multiple scales. Altintas et al. presented an analytical multifrequency method (MF) for the prediction of milling stability lobes [4]. This method requires transfer functions of the structure at the cutter-workpiece contact zone and is not suitable for small radial cutting depth problems. Some of the researches have been focused on the chaotic dynamics beyond the stable region of milling process. For instance, using a 2-DOF tool model, chaotic vibrations in high-speed milling were studied by Banihasan et al. [5]. Also, using a 2-DOF tool model, Moradi et al. predicted the chaotic behavior of the limit cycles in the presence of regenerative chatter for the nonlinear milling process [6]. The averaging method was used by Campa et al. to predict the stability in the milling of thin floors with bull-nose end mills [7]. Using the multistage homotopy perturbation method, Compean et al. investigated the stability of milling process [8]. Peng et al. presented a new method based on dynamic cutting force simulation model and support vector machine to predict chatter stability lobes in milling process [9]. Also, Wan et al. used semi-discretization method to obtain stability lobe diagram in milling process [10]. This method is also used by Wan et al. to predict the lateral and torsional/axial chatter stability in multifunctional tools [11]. Also, Wan et al. established lowest envelop method (LEM) to predict the ultimate stability lobe in milling process by taking the lowest envelop of a group of stability lobes [12]. Transforming the dynamic cutting process into semi-discrete time domain, the stability of the thread milling process was modeled and predicted by Wan and Altintas [13]. Wang et al. utilized Visual C++ software to calculate the chatter stability domain in the high-speed vertical milling during the finish machining of thin-walled workpiece made of titanium alloy [14]. Referencing with the zero order solution, the frequency domain 3-D chatter stability prediction based on the linear and exponential force models are formulated by Yang et al. [15]. Modeling the workpiece-holder system as a 2-DOF system, Qu et al. studied the machining stability in milling of thin-walled plates and developed a 3-D stability lobe diagram of the spindle speed, tool position, and axial depth of cut [16]. Using a 2-DOF tool model, reliability analysis for dynamic structural system was presented by Liu et al. to predict chatter vibration in a milling system based on first-order second-moment method [17]. Also, considering different contact characteristic between milling cutter and workpiece, stability lobe diagrams at different cutter positions are proposed by Yue et al. to predict milling stability by employing full-discrete method [18]. Aiming at process damping caused by interference between a tool flank face and a machined surface of thin-walled part, the dynamic model and critical condition of stability were investigated by Liu et al. using the relative transfer functions [19].

In other researches, internal, primary, sub-, and super harmonic resonances in milling process have been studied. For example, Moradi et al. investigated the occurrence of various types of bifurcation in milling process considering tool wear and process damping [20]. They used 2-DOF linear model for the tool and multiple-scale approach to construct an analytical approximate solutions under primary resonance for this model. They used

similar model to analyze forced vibration of the milling process [21]. They investigated both types of primary and super harmonic resonances while the internal resonance condition exists. In another work, they used a 2-DOF dynamic model including both structural and cutting force nonlinearities to investigate internal resonance and regenerative chatter in milling process [22]. Using 2-DOF model, Nakano et al. investigated the effect of multiple dynamic absorbers on regenerative chatter and resonance caused by forced vibration generated in the end milling operations [23].

In this article, a new model of tool vibration in milling process is presented. Here, we focus on the forced vibration where a 3-D flexible nonlinear model of the cutting tool with including gyroscopic moment and rotary inertia is considered. Equations of motion of the system are obtained using Hamilton's principle. Multiple-scale approach is used to achieve the frequency response of the system in primary, sub-, and super harmonic resonances. Using this analytical solution, the effects of axial depth of cut, cutting tool diameter, cutting tool length, and the number of cutter teeth on the frequency response of the system have been investigated.

2 System model

The cutting tool is modeled as a rotating clamped-free Rayleigh beam as shown in Fig. 1. According to this figure, frame X, Y, Z is an inertial coordinate system and frame x, y, z is a local coordinate system that rotates with a constant rotating speed. It assumes that the tool in start time $t = 0$ is in the direction of a straight line.

Beam bending deflections is shown in Fig. 2. According to Rayleigh beam theory, the components of displacements $u_1(x, y, z, t)$, $u_2(x, y, z, t)$, and $u_3(x, y, z, t)$ from the displacement vector of tool particles with respect to rotating coordinate system may be expressed as:

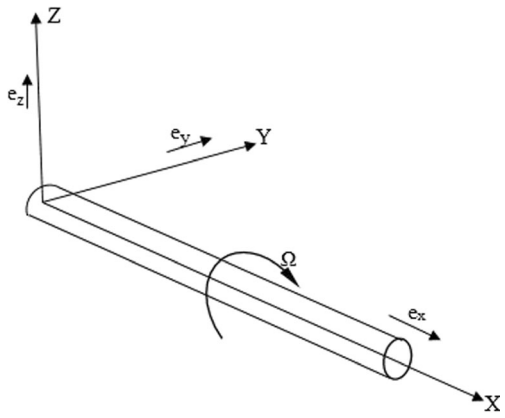

Fig. 1 Undeformed coordinate system [25]

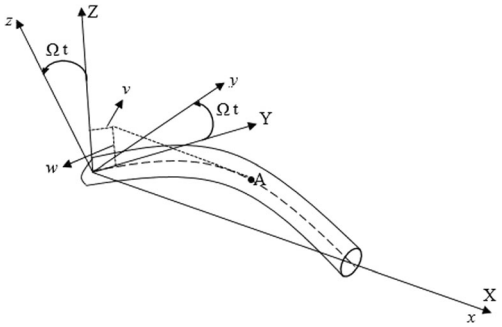

Fig. 2 Deformed beam after elastic displacements [25]

$$\begin{aligned} u_1 &= -z\frac{\partial \overline{w}(x,t)}{\partial x} - y\frac{\partial \overline{v}(x,t)}{\partial x} \\ u_2 &= \overline{v}(x,t) \\ u_3 &= \overline{w}(x,t) \end{aligned} \tag{1}$$

that $\overline{v}$ and $\overline{w}$ show the transformation of the centerline of tool with respect to rotating coordinate. These transformation parameters with respect to rotating coordinate can be calculated by:

$$\begin{aligned} \overline{v} &= v\cos\phi + w\sin\phi \\ \overline{w} &= w\cos\phi - v\sin\phi \end{aligned} \tag{2}$$

where ϕ is the rotation angle of frame x, y, z about X, Y, Z coordinate system with speed of $\phi = \Omega$.

In addition to the moving displacement, the elements of cutting tool have rotating displacement. The relation between the original frame X, Y, Z and the deformed frame x, y, z is described by three sequential Euler angles $\psi_x(x,t)$, $\psi_y(x,t)$ and $\psi_z(x,t)$, as shown in Fig. 3. Because of ignoring the torsional deformation of the tool, one may assume that $\psi_x(x,t) = \Omega t$.

The angular velocity of the deformed frame x, y, z about frame X, Y, Z is [24, 25]:

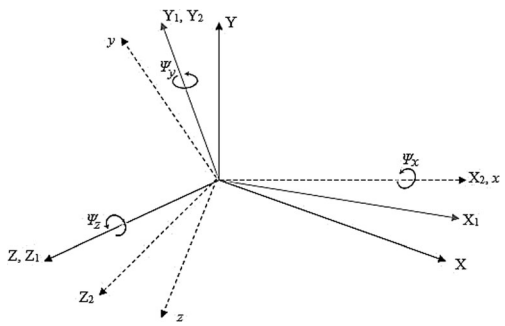

Fig. 3 Coordinate transformations

$$\begin{aligned}\omega &= \omega_1\hat{e}_1 + \omega_2\hat{e}_2 + \omega_3\hat{e}_3\\ &= \left(\Omega - \psi_z \sin\psi_y\right)\hat{e}_1 + \left(\psi_z \cos\psi_y \sin\Omega t + \psi_y \cos\Omega t\right)\hat{e}_2\\ &+ \left(\psi_z \cos\psi_y \cos\Omega t - \psi_y \sin\Omega t\right)\hat{e}_3 \end{aligned} \tag{3}$$

If shear deformation is neglected, angles ψ_z and ψ_y can be related to the displacements as [24, 25]:

$$\begin{aligned}\psi_z &= \sin^{-1}\left[\frac{\frac{\partial v}{\partial x}}{\sqrt{\left(1+\frac{\partial u}{\partial x}\right)^2 + \left(\frac{\partial v}{\partial x}\right)^2}}\right]\\ \psi_y &= -\sin^{-1}\left[\frac{\frac{\partial w}{\partial x}}{\sqrt{\left(1+\frac{\partial u}{\partial x}\right)^2 + \left(\frac{\partial v}{\partial x}\right)^2 + \left(\frac{\partial w}{\partial x}\right)^2}}\right]\end{aligned} \tag{4}$$

3 Equations of motion

In this section, equations of motion of the system are obtained using Hamilton's principle. Hamilton's principle may be expressed as [26]:

$$\int_{t1}^{t2} [\delta(U-T) - \delta W]dt = 0. \tag{5}$$

3.1 Strain energy

The usual expression for strain energy in terms of engineering stresses and strains is:

$$U = \frac{1}{2}\int_0^l \iint_A \left(\sigma_{xx}\varepsilon_{xx} + \sigma_{xy}\varepsilon_{xy} + \sigma_{xz}\varepsilon_{xz}\right) dz\,dy\,dx \tag{6}$$

Where

$$\begin{aligned}\sigma_{xx} &= E\varepsilon_{xx}\\ \sigma_{xy} &= G\varepsilon_{xy}\\ \sigma_{xz} &= G\varepsilon_{xz}\end{aligned} \tag{7}$$

The variation of strain energy yields:

$$\delta U = \int_0^l \left(\overline{Y}_v \delta v + \overline{Y}_w \delta w\right)dx + b(U) \tag{8}$$

where

$$\begin{aligned}\overline{Y}_v &= \left(M_{z'}\right)'' - \left(V_{x'}v'\right)'\\ \overline{Y}_w &= \left(-M_{y'}\right)'' - \left(V_{x'}w'\right)'\end{aligned} \tag{9}$$

and

$$\begin{aligned}b(U) = &\left[V_{x'}v' - \left(M_{z'}\right)'\right]\delta v\Big|_0^l + \left(M_{z'}\right)\delta v'\Big|_0^l\\ &+ \left(-M_{y'}\right)\delta w'\Big|_0^l + \left[V_{x'}w' - \left(-M_{y'}\right)'\right]\delta w\Big|_0^l\end{aligned} \tag{10}$$

where the resultant stress and moments are defined by:

$$\begin{aligned}V_{x'} &= \iint_A \sigma_{xx}\mathrm{d}y\mathrm{d}z = {}^{EA}/_2\left(v'^2 + w'^2\right)\\ M_{y'} &= EI_{y'}\left(-w''\right)\\ M_{z'} &= EI_{z'}\left(v''\right)\end{aligned} \tag{11}$$

The section integrals in Eq. (11) are defined as follows:

$$\begin{aligned}A &= \iint_A \mathrm{d}y\mathrm{d}z = \pi R^2\\ I_{y'} &= \iint_A z^2\mathrm{d}y\mathrm{d}z = {}^{\pi}/_4 R^4\\ I_{z'} &= \iint_A y^2\mathrm{d}y\mathrm{d}z = {}^{\pi}/_4 R^4\end{aligned} \tag{12}$$

3.2 Kinetic energy

The kinetic energy of cutting tool is calculated as follow [24, 25]:

$$\begin{aligned}T &= T_{\text{tran}} + T_{rot}\\ &= \frac{1}{2}\int_0^L \int_A \rho\,\dot{r}\cdot\dot{r}\,dA\,dx + \frac{1}{2}\int_0^L \int_A \rho\{\omega\}^T[I]\{\omega\}dA\,dx\\ &= \frac{1}{2}\int_0^L \left[\rho A\left(\dot{v}^2 + \dot{w}^2\right) + \rho J\,\omega_1^2 + \rho I\,\left(\omega_2^2 + \omega_3^2\right)\right]dx\end{aligned} \tag{13}$$

where

$$J = \iint_A \left(y^2 + z^2\right)\mathrm{d}y\mathrm{d}z = {}^{\pi}/_2 R^4 \tag{14}$$

For small deformations, the displacement components and the variation of them with respect to x is so small. Therefore, the magnitudes of ψ_z and ψ_y are small and can be approximated by $\partial v/\partial x$ and $-\partial w/\partial x$, respectively. So the kinetic energy of system is equal to:

$$T = \frac{1}{2}\int_0^L \left[\rho A\left(\dot{v}^2 + \dot{w}^2\right) + \rho I\left(4\omega\frac{\partial\dot{v}}{\partial x}\frac{\partial w}{\partial x} + \left(\frac{\partial\dot{v}}{\partial x}\right)^2 + \left(\frac{\partial\dot{w}}{\partial x}\right)^2\right) + \rho J\,\Omega^2\right]dx \tag{15}$$

The variation of strain energy yields:

$$\delta T = \int_O^L \left[\left(\overline{z_v}\right)\delta v + \left(\overline{z_w}\right)\delta w\right]dx + b(T) \tag{16}$$

in which:

$$\begin{aligned}\overline{z_v} &= -\mathrm{m}\ddot{v} + \frac{mR^2}{2}\left(\ddot{v}'' + 2\Omega\dot{w}''\right)\\ \overline{z_w} &= -\mathrm{m}\ddot{w} + \frac{mR^2}{2}\left(\ddot{w}'' - 2\Omega\dot{v}''\right)\end{aligned} \tag{17}$$

$$\begin{aligned}b(T) = {} & \frac{mR^2}{4}\left(\ddot{v}' + 2\Omega\dot{w}'\right)\delta v\Big|_o^L\\ & + \frac{mR^2}{4}\left(\ddot{w}' - 2\Omega\dot{v}'\right)\delta w\Big|_o^L\end{aligned} \tag{18}$$

3.3 Virtual work of the nonconservative forces

The virtual work δW of the nonconservative forces may be expressed as:

$$\delta W = \int_0^l \left(L_v\delta v + L_w\delta w\right)dx \tag{19}$$

where

$$\begin{aligned}L_v &= F_f\delta_D(x - x_0)\\ L_w &= F_t\delta_D(x - x_0)\end{aligned} \tag{20}$$

Cutting force in radial (F_r) and tangential (F_t) directions can be obtained by [22, 27]:

$$\begin{aligned}F_r = {} & \left(-\frac{N}{2\pi}\left[\alpha_0(v(x,t) - v(x,t-\tau)) + \beta_0(w(x,t) - w(x,t-\tau)) + \gamma_0\right)+\right.\\ & \left.\left(-\frac{c_f}{2}[\zeta_1\cos(2\Omega t - \pi/2) - \eta_1\cos 2\Omega t + \eta_1] - \eta_2\cos(\Omega t - \pi/2) - \zeta_2\cos\Omega t\right)\right.\\ F_t = {} & \left(\frac{N}{2\pi}\left[\alpha'_0(v(x,t) - v(x,t-\tau)) + \beta'_0(w(x,t) - w(x,t-\tau)) + \gamma'_0\right)+\right.\\ & \left.\left(-\frac{c_f}{2}[\eta_1\cos(2\Omega t - \pi/2) + \zeta_1\cos 2\Omega t - \zeta_1] + \zeta_2\cos(\Omega t - \pi/2) - \eta_2\cos\Omega t\right)\right.\end{aligned} \tag{21}$$

where $\tau = 2\pi/N\Omega$.

For half immersion up-milling, the coefficients of Eqs. (21) are specified as:

$$\begin{aligned}\alpha_0 &= 0.5\xi_1 + 0.25\pi\eta_1 & \alpha'_0 &= -0.5\eta_1 + 0.25\pi\xi_1\\ \beta_0 &= 0.5\eta_1 + 0.25\pi\xi_1 & \beta'_0 &= 0.5\xi_1 - 0.25\pi\eta_1\\ \gamma_0 &= \eta_2 + \xi_2 & \gamma'_0 &= \xi_2 - \eta_2\end{aligned} \tag{22}$$

where the parameters $\xi_1, \xi_2, \eta_1, \eta_2$ are equal to:

$$\begin{aligned}\xi_1 &= k_{tc}a & \xi_2 &= k_{te}a\\ \eta_1 &= k_{rc}a & \eta_2 &= k_{re}a\end{aligned} \tag{23}$$

Substituting Eq. (8), Eq. (16), and Eq. (19) in Eq. (5), equations of motion in two directions y and z can be derived as:

$$\begin{aligned}EI\left(v''\right)'' - {}^{EA}/_2\left[\left(v'^2 + w'^2\right)v'\right]' + m\ddot{v} - 2\rho I\Omega\dot{w}'' - \rho I\ddot{v}'' &= F_r\delta_D(x - x_o)\\ EI\left(w''\right)'' - {}^{EA}/_2\left[\left(v'^2 + w'^2\right)w'\right]' + m\ddot{w} + 2\rho I\Omega\dot{v}'' - \rho I\ddot{w}'' &= F_t\delta_D(x - x_o)\end{aligned} \tag{24}$$

In Eq. (24), the terms $2\rho I\Omega\dot{w}''$ and $2\rho I\Omega\dot{v}''$ appear because of the gyroscopic moment, and the terms $\rho I\ddot{v}''$ and $\rho I\ddot{w}''$ appear because of the rotary inertia [28].

4 Solution of equations of motion

For the Eq. (24), the deflection fields $v(x,t)$ and $w(x,t)$ can be assumed as follows:

$$\begin{aligned}v(x,t) &= \sum_{i=1}^{n} V_i(x)T_{vi}(t)\\ w(x,t) &= \sum_{i=1}^{n} W_i(x)T_{wi}(t)\end{aligned} \tag{25}$$

where $V_i(x)$and $W_i(x)$ are the mode functions of the cutting tool in y and z directions, respectively; $T_{vi}(t)$and $T_{wi}(t)$are the generalized coordinates in terms of time t; and n is the total mode numbers of the tool mode functions selected for the calculation. The cutting tool boundary conditions are considered as follow:

$$\begin{aligned}&v(0,t) = 0, \quad \frac{\partial v(0,t)}{\partial x} = 0, \quad \frac{\partial^2 v(l,t)}{\partial x^2} = 0, \quad \frac{\partial^3 v(l,t)}{\partial x^3} = 0\\ &\mathrm{w}(0,t) = 0, \quad \frac{\partial w(0,t)}{\partial x} = 0, \quad \frac{\partial^2 w(l,t)}{\partial x^2} = 0, \quad \frac{\partial^3 w(l,t)}{\partial x^3} = 0\end{aligned} \tag{26}$$

According to reference [29], the following shape functions are selected for cutting tool:

$$V_i(x) = W_i(x) = cos\beta_i(x) - cosh\beta_i(x) - \frac{\cos\beta_i\cdot l + \cosh\beta_i\cdot l}{\sin\beta_i\cdot l + \sinh\beta_i\cdot l}\left(\sin\beta_i(x) - \sinh\beta_i(x)\right) \tag{27}$$

in which for the first three modes of vibration, $\beta_i$is equal to:

$$\beta_1 l = 1.875, \quad \beta_2 l = 4.691, \quad \beta_3 l = 7.8547 \tag{28}$$

After substituting Eq. (25) into Eq. (24) and multiplying resultant equations by $V_i(x)$and $W_i(x)$, respectively, and then applying integral over the tool length, yields the second-order ordinary differential equations of the tool lateral vibration in terms of the unknown time-dependent functions $T_{vi}(t)$and $T_{wi}(t)$as follows:

$$A_{1i}T_{vi}(t)+A_{2i}T_{vi}{}^3(t)+A_{3i}T_{vi}(t)T_{wi}{}^2(t)+A_{4i}T_{wi}(t)+A_{5i}\ddot{T}_{vi}(t)=A_{6i}(T_{vi}(t)-T_{vi}(t-\tau))+A_{7i}(T_{wi}(t)-T_{wi}(t-\tau))+A_{8i}+A_{9i}(-\frac{c_f}{2}[\zeta_1\cos(2\Omega t-\pi/2)-\eta_1\cos 2\Omega t]-\eta_2\cos(\Omega t-\pi/2)-\zeta_2\cos\Omega t)$$
$$B_{1i}T_w(t)+B_{2i}T_{wi}{}^3(t)+B_{3i}T_{wi}(t)T_w{}^2(t)+B_{4i}T_{vi}(t)+B_{5i}\ddot{T}_{wi}(t)=B_{6i}(T_{vi}(t)-T_{vi}(t-\tau))+B_{7i}(T_{wi}(t)-T_{wi}(t-\tau))+B_{8i}+B_{9i}\left(-\frac{c_f}{2}\left[\eta_1\cos\left(2\Omega t-\pi/2\right)+\zeta_1\cos 2\Omega t\right]+\zeta_2\cos\left(\Omega t-\pi/2\right)-\eta_2\cos\Omega t\right) \quad (29)$$

The coefficients of Eq. (29) are presented in "Appendix A".

5 Perturbation analysis of the process

In this section, the multiple-scale approach is used to find the frequency response for the milling process in primary and super harmonic resonances. In this method, an expansion representing the response to be a function of multiple-independent scales is used, where ε is a small parameter representing the time scale [30]. Accordingly, derivatives with respect to t become expansions in terms of the partial derivatives with respect to independent scales as:

$$\frac{d}{dt}=D_0+\varepsilon D_1+\varepsilon^2 D_2+\ldots$$
$$\frac{d^2}{dt^2}=D_0^2+2\varepsilon D_0D_1+\varepsilon^2\left(D_1^2+2D_0D_2\right)+\ldots \quad (30)$$

in which

$$D_i=\frac{d}{dT_i},\quad T_i=\varepsilon^i t,\quad \mathrm{i}=1,2,3,\ldots \quad (31)$$

Solution of Eq. (29) can be written in the expansion form as:

$$T_{vi}(t,\varepsilon)=q_i(t,\varepsilon)=q_{0i}(T_0,T_1,T_2,\ldots)+\varepsilon q_{1i}(T_0,T_1,T_2,\ldots)+\varepsilon^2 q_{2i}(T_0,T_1,T_2,\ldots)+\ldots$$
$$T_{wi}(t,\varepsilon)=p_i(t,\varepsilon)=p_{0i}(T_0,T_1,T_2,\ldots)+\varepsilon p_{1i}(T_0,T_1,T_2,\ldots)+\varepsilon^2 p_{2i}(T_0,T_1,T_2,\ldots)+\ldots \quad (32)$$

Case 1: Nonresonant excitation

In this case, with substituting Eqs. (30)–(32) into Eq. (29) and equating coefficients of similar powers of $\varepsilon$to zero and neglecting powers of εthat are more than 2, we obtain:

$$\varepsilon^0:\ \begin{aligned}&D_0^2q_{0i}+A'_{4i}D_0p_{0i}+A'_{1i}q_{0i}=\\&A'_{8i}+A'_{9i}\left(-\frac{c_f}{2}[\zeta_1\cos(2\Omega t-\pi/2)-\eta_1\cos 2\Omega t]-\eta_2\cos(\Omega t-\pi/2)-\zeta_2\cos\Omega t\right)\\&D_0^2p_{0i}+B'_{4i}D_0q_{0i}+B'_{1i}p_{0i}=\\&B'_{8i}+B'_{9i}\left(-\frac{c_f}{2}[\eta_1\cos(2\Omega t-\pi/2)+\zeta_1\cos 2\Omega t]+\zeta_2\cos(\Omega t-\pi/2)-\eta_2\cos\Omega t\right)\end{aligned} \quad (33)$$

$$\varepsilon^1:\ \begin{aligned}&D_0^2q_{1i}+A'_{4i}D_0p_{1i}+A'_{1i}q_{1i}=\\&-2D_1D_0q_{0i}-A'_4D_1p_{0i}+A''_6(q_{0i}-q_{0i\tau})+A''_7(p_{0i}-p_{0i\tau})-A''_{2i}q_{0i}{}^3-A''_{3i}p_{0i}{}^2q_{0i}\\&D_0^2p_{1i}+B'_4D_0q_{1i}+B'_{1i}p_{1i}=\\&-2D_1D_0p_{0i}-B'_{4i}D_1q_{0i}+B''_{6i}(q_{0i}-q_{0i\tau})+B''_{7i}(p_{0i}-p_{0i\tau})-B''_{2i}p_{0i}{}^3-B''_{3i}q_{0i}{}^2p_{0i}\end{aligned} \quad (34)$$

where $A'_i=A_i/A_{5i}$, $B'_i=B_i/B_{5i}$, $A''_i=\varepsilon A'_i$, $B''_i=\varepsilon B'_i$, $p_{i\tau}=p_i(t-\tau)$, and $q_{i\tau}=q_i(t-\tau)$.

Solution of Eq. (33) can be expressed in the form

$$\begin{aligned}q_{0i}&=C_1(T_1)\exp(i\omega_1T_0)+C_2(T_1)\exp(i\omega_2T_0)+\frac{A'_{8i}}{A'_{1i}}+P_1\cos(2\Omega t-\pi/2)\\&+P_2\cos 2\Omega t+P_3\cos(\Omega t-\pi/2)+P_4\cos\Omega t+cc\\p_{0i}&=\Lambda_1C_1(T_1)\exp(i\omega_1T_0)+\Lambda_2C_2(T_1)\exp(i\omega_2T_0)+\frac{B'_{8i}}{B'_{1i}}+P_5\cos(2\Omega t-\pi/2)\\&+P_6\cos 2\Omega t+P_7\cos(\Omega t-\pi/2)+P_8\cos\Omega t+cc\end{aligned} \quad (35)$$

where cc stands for the complex conjugate of the preceding terms, C_1 and C_2 are arbitrary functions at this level of approximation, and $\Lambda_n=-\frac{i\omega_nB'_{4i}}{B'_{1i}-\omega_n^2}$, in which:

$$\omega_1=\frac{\sqrt{\left(A'_{1i}+B'_{1i}-A'_{4i}B'_{4i}\right)-\sqrt{\left(A'_{1i}+B'_{1i}-A'_{4i}B'_{4i}\right)^2-4A'_{1i}B'_{1i}}}}{2}$$
$$\omega_2=\frac{\sqrt{\left(A'_{1i}+B'_{1i}-A'_{4i}B'_{4i}\right)+\sqrt{\left(A'_{1i}+B'_{1i}-A'_{4i}B'_{4i}\right)^2-4A'_{1i}B'_{1i}}}}{2} \quad (36)$$

The coefficients of P_1 to P_8 are presented in "Appendix B".

Substituting q_0 and p_0 into Eq. (34), the solvability condition yields:

$$R_{11}+\overline{\Lambda}_1R_{21}=0,\quad R_{12}+\overline{\Lambda}_1R_{22}=0 \quad (37)$$

where R_{11} and R_{12} are the coefficient of terms $\exp(i\omega_1T_0)$ and $\exp(i\omega_2T_0)$ in the first equation of motion and R_{21} and $R_{22}$are the coefficient of terms $\exp(i\omega_1T_0)$ and $\exp(i\omega_2T_0)$ in the second equation of motion.

Separating real and imaginary parts in Eq. (37) and using λ_r as real and λ_i as imaginary parts, Eq. (37) can be written as:

$$\begin{aligned}&(\lambda_{1r}+i\lambda_{1i})C_1+(\lambda_{2r}+i\lambda_{2i})C_1+(\lambda_{3r}+i\lambda_{3i})C_1C_2\overline{C}_2+(\lambda_{4r}+i\lambda_{4i})C_1^2\overline{C}_1=0\\&(\lambda_{5r}+i\lambda_{5i})C_2+(\lambda_{6r}+i\lambda_{6i})C_2+(\lambda_{7r}+i\lambda_{7i})C_1C_2\overline{C}_1+(\lambda_{8r}+i\lambda_{8i})C_2^2\overline{C}_2=0\end{aligned} \quad (38)$$

Coefficients of Eq. (38) are presented in "Appendix C".

Putting:

$$C_1=0.5f_1\exp(i\theta_1)$$
$$C_2=0.5f_2\exp(i\theta_2) \quad (39)$$

in Eq. (38) and separating real and imaginary parts, the amounts of C_1 and C_2will be achieved. Substituting C_1andC_2into Eq. (35), the response of the system can be written as follows:

$$
\begin{aligned}
q_i &= 0.5 f_{10}\exp\left(\frac{-\lambda_{2i}}{\lambda_{1i}}t\right)\exp\left(i\left(\frac{\lambda_{2r}}{\lambda_{1i}}t-\frac{\lambda_{3r}\lambda_{5i}}{8\lambda_{1i}\lambda_{6i}}{f_{20}}^2\exp\left(\frac{-2\lambda_{6i}}{\lambda_{5i}}t\right)-\frac{\lambda_{4r}\lambda_{1i}}{8\lambda_{1i}\lambda_{2i}}{f_{10}}^2\exp\left(\frac{-2\lambda_{2i}}{\lambda_{1i}}t\right)+\theta_{10}\right)\right)\\
&\exp(i w_1 t)\\
&+0.5 f_{20}\exp\left(\frac{-\lambda_{6i}}{\lambda_{5i}}t\right)\exp\left(i\left(\frac{\lambda_{6r}}{\lambda_{5i}}t-\frac{\lambda_{7r}\lambda_{1i}}{8\lambda_{5i}\lambda_{2i}}{f_{10}}^2\exp\left(\frac{-2\lambda_{2i}}{\lambda_{1i}}t\right)-\frac{\lambda_{8r}\lambda_{5i}}{8\lambda_{5i}\lambda_{6i}}{f_{20}}^2\exp\left(\frac{-2\lambda_{6i}}{\lambda_{5i}}t\right)+\theta_{20}\right)\right)\\
&\exp(i w_2 t)+cc\\
&+\frac{A_{8i}}{A_{1i}}+P_1\cos\left(2\Omega t-\pi/2\right)+P_2\cos 2\Omega t+P_3\cos\left(\Omega t-\pi/2\right)+P_4\cos\Omega t\\
p_i &= 0.5\Lambda_1 f_{10}\exp\left(\frac{-\lambda_{2i}}{\lambda_{1i}}t\right)\exp\left(i\left(\frac{\lambda_{2r}}{\lambda_{1i}}t-\frac{\lambda_{3r}\lambda_{5i}}{8\lambda_{1i}\lambda_{6i}}{f_{20}}^2\exp\left(\frac{-2\lambda_{6i}}{\lambda_{5i}}t\right)-\frac{\lambda_{4r}\lambda_{1i}}{8\lambda_{1i}\lambda_{2i}}{f_{10}}^2\exp\left(\frac{-2\lambda_{2i}}{\lambda_{1i}}t\right)+\theta_{10}\right)\right)\\
&\exp(i w_1 t)\\
&+0.5\Lambda_2 f_{20}\exp\left(\frac{-\lambda_{6i}}{\lambda_{5i}}t\right)\exp\left(i\left(\frac{\lambda_{6r}}{\lambda_{5i}}t-\frac{\lambda_{7r}\lambda_{1i}}{8\lambda_{5i}\lambda_{2i}}{f_{10}}^2\exp\left(\frac{-2\lambda_{2i}}{\lambda_{1i}}t\right)-\frac{\lambda_{8r}\lambda_{5i}}{8\lambda_{5i}\lambda_{6i}}{f_{20}}^2\exp\left(\frac{-2\lambda_{6i}}{\lambda_{5i}}t\right)+\theta_{20}\right)\right)\\
&\exp(i w_2 t)+cc\\
&+\frac{B_{8i}}{B_{1i}}+P_5\cos\left(2\Omega t-\pi/2\right)+P_6\cos 2\Omega t+P_7\cos\left(\Omega t-\pi/2\right)+P_8\cos\Omega t
\end{aligned}
\tag{40}
$$

In this paper, both types of primary and super harmonic resonances are investigated. For this reason, some parameters of Eq. (29) have been replaced with following expressions:

$$
\begin{aligned}
&A_{2i}=\varepsilon A_{2i},\ \ A_{3i}=\varepsilon A_{3i},\ \ A_{6i}=\varepsilon A_{6i},\ \ A_{7i}=\varepsilon A_{7i},\ \ A_{9i}=\varepsilon A_{9i}\\
&B_{2i}=\varepsilon B_{2i},\ \ B_{3i}=\varepsilon B_{3i},\ \ B_{6i}=\varepsilon B_{6i},\ \ B_{7i}=\varepsilon B_{7i},\ \ B_{9i}=\varepsilon B_{9i}
\end{aligned}
\tag{41}
$$

Case 2: Primary resonance, $\Omega=\omega_1$

In this case, to express the nearness of Ω to ω_1 quantitatively, detuning parameter σ is introduced as:

$$\Omega=\omega_1+\varepsilon\sigma \tag{42}$$

Substituting Eqs. (30)–(32) and (41)–(42) into Eq. (29) and equating coefficients of like powers of ε to zero, we obtain:

$$
\varepsilon^0:\ \begin{aligned}
&D_0^2 q_{0i}+A'_{4i}D_0 p_{0i}+A'_{1i}q_{0i}=A'_{8i}\\
&D_0^2 p_{0i}+B'_{4i}D_0 q_{0i}+B'_{1i}p_{0i}=B'_{8i}
\end{aligned}
\tag{43}
$$

$$
\varepsilon^1:\ \begin{aligned}
&D_0^2 q_{1i}+A'_{4i}D_0 p_{1i}+A'_{1i}q_{1i}=-2D_1D_0q_{0i}-A'_{4i}D_1p_{0i}+A'_{6i}(q_{0i}-q_{0i\tau})+A'_{7i}(p_{0i}-p_{0i\tau})-A'_{2i}{q_{0i}}^3-A'_{3i}{p_{0i}}^2q_{0i}\\
&\quad+A'_{9i}\left(\frac{c_f}{2}[\zeta_1\cos(2\Omega t-\pi/2)-\eta_1\cos 2\Omega t]-\eta_2\cos(\Omega t-\pi/2)-\zeta_2\cos\Omega t\right)\\
&D_0^2 p_{1i}+B'_{4i}D_0 q_{1i}+B'_{1i}p_{1i}=-2D_1D_0p_{0i}-B'_{4i}D_1q_{0i}+B'_{6i}(q_{0i}-q_{0i\tau})+B'_{7i}(p_{0i}-p_{0i\tau})-B'_{2i}{p_{0i}}^3-B'_{3i}{q_{0i}}^2p_{0i}\\
&\quad+B'_{9i}\left(\frac{c_f}{2}[\eta_1\cos(2\Omega t-\pi/2)+\zeta_1\cos 2\Omega t]+\zeta_2\cos(\Omega t-\pi/2)-\eta_2\cos\Omega t\right)
\end{aligned}
\tag{44}
$$

The solution of Eq. (43) can be expressed in the form

$$
\begin{aligned}
q_{0i} &= C_1(T_1)\exp(i\omega_1T_0)+C_2(T_1)\exp(i\omega_2T_0)+\frac{A'_{8i}}{A'_{1i}}+cc\\
p_{0i} &= \Lambda_1C_1(T_1)\exp(i\omega_1T_0)+\Lambda_2C_2(T_1)\exp(i\omega_2T_0)+\frac{B'_{8i}}{B'_{1i}}+cc
\end{aligned}
\tag{45}
$$

After substituting Eq. (45) into Eq. (34), the solvability condition yields that:

$$R_{11}+\overline{\Lambda}_1R_{21}=0,\ \ R_{12}+\overline{\Lambda}_1R_{22}=0 \tag{46}$$

where R_{11} and R_{12} are coefficient of terms $\exp(i\omega_1T_0)$ and $\exp(i\omega_2T_0)$ in the first equation of motion and R_{21} and $R_{22}$are, respectively, coefficient of terms $\exp(i\omega_1T_0)$ and $\exp(i\omega_2T_0)$ in the second equation of motion.

Separating real and imaginary parts in Eq. (45), using λ_r as real part and λ_i as imaginary part, we obtain:

$$
\begin{aligned}
&(\lambda_{1r}+i\lambda_{1i})C_1+(\lambda_{2r}+i\lambda_{2i})C_1+(\lambda_{3r}+i\lambda_{3i})C_1C_2\overline{C}_2+(\lambda_{4r}+i\lambda_{4i})C_1^2\overline{C}_1+\frac{1}{2}\left(\left(A'_{9i}\eta_2+i\overline{\Lambda}_1B'_{9i}\eta_2\right)\sin(\sigma T_1)\right.\\
&\left.+\left(A'_{9i}\zeta_2+B'_{9i}i\overline{\Lambda}_1\zeta_2\right)\cos(\sigma T_1)\right)+i\left(\frac{1}{2}\left(\left(-A'_{9i}\eta_2-i\overline{\Lambda}_1B'_{9i}\eta_2\right)\cos(\sigma T_1)+\left(A'_{9i}\zeta_2+B'_{9i}i\overline{\Lambda}_1\zeta_2\right)\cos(\sigma T_1)\right)=0\\
&(\lambda_{5r}+i\lambda_{5i})C_2+(\lambda_{6r}+i\lambda_{6i})C_2+(\lambda_{7r}+i\lambda_{7i})C_1C_2\overline{C}_1+(\lambda_{8r}+i\lambda_{8i})C_2^2\overline{C}_2=0
\end{aligned}
\tag{47}
$$

Putting:

$$
\begin{aligned}
C_1 &= 0.5 f_1\exp(i\theta_1)\\
C_2 &= 0.5 f_2\exp(i\theta_2)
\end{aligned}
\tag{48}
$$

$$\sigma T_1-\beta=\upsilon \tag{49}$$

into Eq. (47) and separating real and imaginary part, for steady state condition, we have:

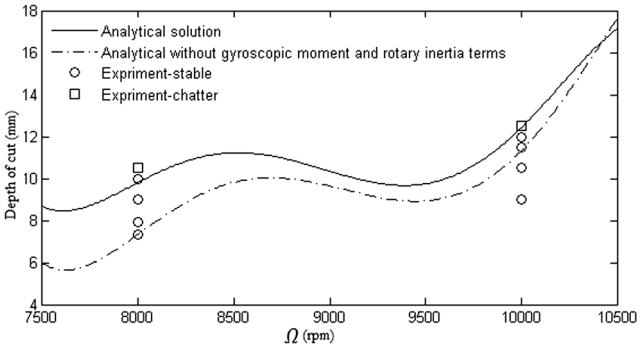

Fig. 4 Computational and experimentally measured stability limit

$$\sigma = \frac{1}{\lambda_{1i}}\left(\lambda_{2r} + \frac{1}{4}\lambda_{5r}{f_1}^2 \pm \sqrt{\frac{\left(A'_{9i}\eta_2 + i\overline{\Lambda}_1 B'_{9i}\eta_2\right)^2 + \left(A'_{9i}\zeta_2 + i\overline{\Lambda}_1 B'_{9i}\zeta_2\right)^2}{{f_1}^2} - \lambda_{2i}^2}\right) \tag{50}$$

Equation (50) that is frequency response function is an implicit equation for the amplitude of the response f_1 as a function of the detuning parameter σ.

Case 3: Primary resonance, $\Omega = \omega_2$

Similar to case 1, for this case, the frequency response function can be expressed as follows:

$$\sigma = \frac{1}{\lambda_{5i}}\left(\lambda_{6r} + \frac{1}{4}\lambda_{1r}{f_2}^2 \pm \sqrt{\frac{\left(A'_{9i}\eta_2 + i\overline{\Lambda}_1 B'_{9i}\eta_2\right)^2 + \left(A'_{9i}\zeta_2 + i\overline{\Lambda}_1 B'_{9i}\zeta_2\right)^2}{{f_2}^2} - \lambda_{6i}^2}\right) \tag{51}$$

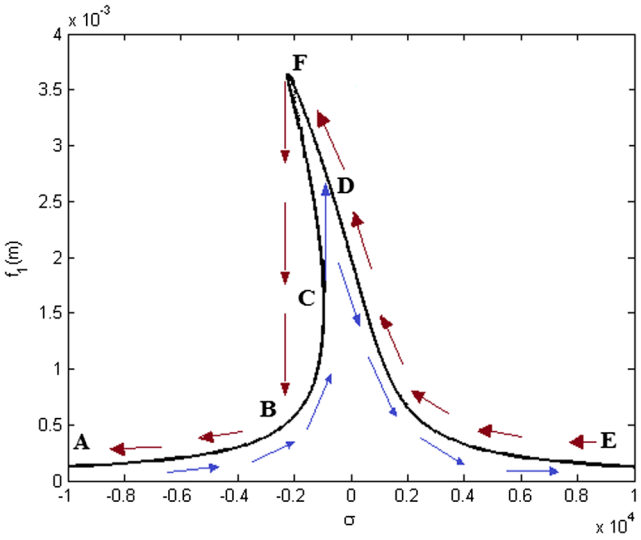

Fig. 5 Frequency response of the tool tip vibration for the primary resonance case ($\Omega = \omega_1$)

Equation (51) represents the amplitude of the response f_2 as a function of the detuning parameter σ.

Case 4: Super harmonic resonance, $2\Omega = \omega_1$

In this case, detuning parameter σ is introduced as:

$$2\Omega = \omega_1 + \varepsilon\sigma \tag{52}$$

With substituting Eqs. (30)–(32) and (52) in Eq. (29) and equating coefficients of like powers of ε to zero, we obtain:

$$\varepsilon^0: \begin{array}{l} D_0^2 q_{0i} + A'_{4i} D_0 p_{0i} + A'_{1i} q_{0i} = A'_{8i} + A'_{9i}\left(-\frac{c_f}{2}[\zeta_1 \cos(2\Omega t - \pi/2) - \eta_1 \cos 2\Omega t] - \eta_2 \cos(\Omega t - \pi/2) - \zeta_2 \cos\Omega t\right) \\ D_0^2 p_{0i} + B'_{4i} D_0 q_{0i} + B'_{1i} p_{0i} = B'_{8i} + B'_{9i}\left(-\frac{c_f}{2}[\eta_1 \cos(2\Omega t - \pi/2) + \zeta_1 \cos 2\Omega t] + \zeta_2 \cos(\Omega t - \pi/2) - \eta_2 \cos\Omega t\right) \end{array} \tag{53}$$

$$\varepsilon^1: \begin{array}{l} D_0^2 q_{1i} + A'_{4i} D_0 p_{1i} + A'_{1i} q_{1i} = -2D_1 D_0 q_{0i} - A'_{4i} D_1 p_{0i} + A''_{6i}(q_{0i} - q_{0i\tau}) + A''_{7i}(p_{0i} - p_{0i\tau}) - A''_{2i} {q_{0i}}^3 - A''_{3i} {p_{0i}}^2 q_{0i} \\ D_0^2 p_{1i} + B'_{4i} D_0 q_{1i} + B'_{1i} p_{1i} = -2D_1 D_0 p_{0i} - B'_{4i} D_1 q_{0i} + B''_{6i}(q_{0i} - q_{0i\tau}) + B''_{7i}(p_{0i} - p_{0i\tau}) - B''_{2i} {p_{0i}}^3 - B''_{3i} {q_{0i}}^2 p_{0i} \end{array} \tag{54}$$

Table 1 Main simulation parameters for a milling process

Parameters	Value	Parameters	Value
E	2×10^{11} Pa	x_0	0.13 m
ρ	7850 Kg.m^{-3}	ξ_1	620 N/mm
l	0.13 m	ξ_2	43 N
d	8 mm	η_1	208 N/mm
N	4	η_2	52 N
c_f	0.2 mm/rev − tooth		

The solution of Eq. (53) can be expressed as

$$\begin{array}{l} q_{0i} = C_1(T_1)\exp(i\omega_1 T_0) + C_2(T_1)\exp(i\omega_2 T_0) + \frac{A'_{8i}}{A'_{1i}} + P_1\cos(2\Omega t - \pi/2) \\ + P_2\cos 2\Omega t + P_3\cos(\Omega t - \pi/2) + P_4\cos\Omega t + cc \\ p_{0i} = \Lambda_1 C_1(T_1)\exp(i\omega_1 T_0) + \Lambda_2 C_2(T_1)\exp(i\omega_2 T_0) + \frac{B'_{8i}}{B'_{1i}} + P_5\cos(2\Omega t - \pi/2) \\ + P_6\cos 2\Omega t + P_7\cos(\Omega t - \pi/2) + P_8\cos\Omega t + cc \end{array} \tag{55}$$

Similar to case 2, we can obtain that:

$$\sigma = \frac{1}{\lambda_{1i}}\left(\lambda_{2r} + \frac{1}{4}\lambda_{5r}{f_1}^2 \pm \sqrt{\frac{\left(A'_{9i}\frac{c_f}{2}\eta_1 + i\overline{\Lambda}_1 B'_{9i}\frac{c_f}{2}\eta_1\right)^2 + \left(A'_{9i}\frac{c_f}{2}\zeta_1 + i\overline{\Lambda}_1 B'_{9i}\frac{c_f}{2}\zeta_1\right)^2}{{f_1}^2} - \lambda_{2i}^2}\right) \tag{56}$$

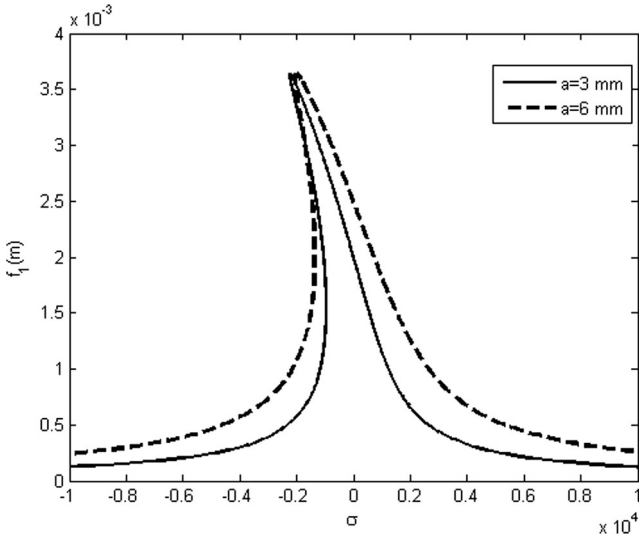

Fig. 6 The effect of axial depth of cut on the frequency response of the tool tip vibration for the primary resonance case ($\Omega = \omega_1$)

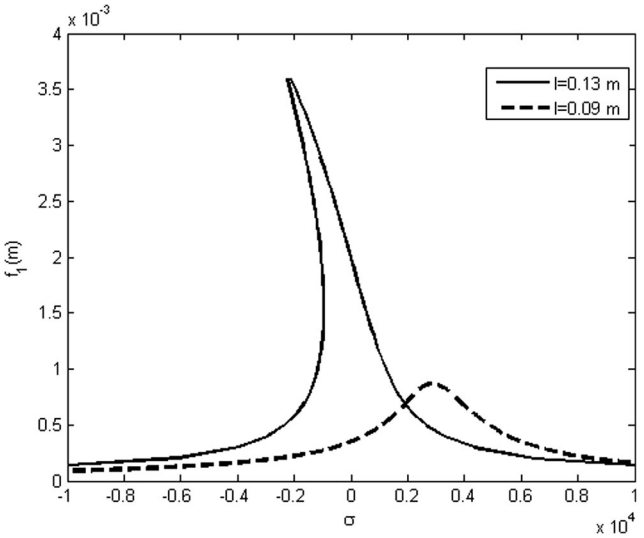

Fig. 8 The effect of cutting tool length on the frequency response of the tool tip vibration for the primary resonance case ($\Omega = \omega_1$)

Case 5: Super harmonic resonance, $2\Omega = \omega_2$

Similar to case 4, the frequency response function for this case can be determined as follows:

$$\sigma = \frac{1}{\lambda_{5i}}\left(\lambda_{6r} + \frac{1}{4}\lambda_{1r}{f_2}^2 \pm \sqrt{\frac{\left(A'_{9i}\frac{c_f}{2}\eta_1 + i\overline{\Lambda}_1 B'_{9i}\frac{c_f}{2}\eta_1\right)^2 + \left(A'_{9i}\frac{c_f}{2}\zeta_1 + i\overline{\Lambda}_1 B'_{9i}\frac{c_f}{2}\zeta_1\right)^2}{{f_2}^2} - \lambda_{6i}^2}\right) \quad (57)$$

6 Simulations, results, and discussion

6.1 Validation of the model

To validate the model presented in this paper, its predictions of the system stability are compared with the experimental results reported by Moradi et al. [31]. In this reference, the stability lobes diagram for a milling process has been investigated experimentally. The results for two spindle speeds of $\Omega = 8000$ and 10000 rpm are presented in Fig. 4. Using the basic parameters presented in reference [31] and the solution method of this paper, stability diagram for the milling process has been constructed using the following process:

1. For special tool rotational speed, time response of the system for different depth of cut (a) has been plotted.
2. The first depth of cut in which the process is unstable is the border between stable and unstable process and specified in the stability diagram by a point.

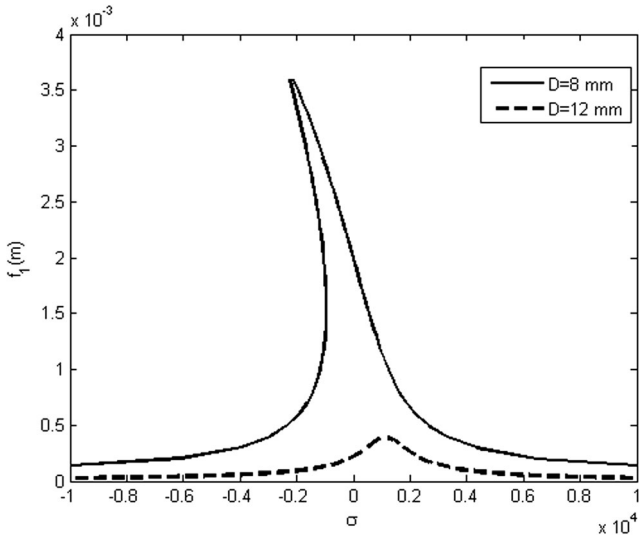

Fig. 7 The effect of cutting tool diameter on the frequency response of the tool tip vibration for the primary resonance case ($\Omega = \omega_1$)

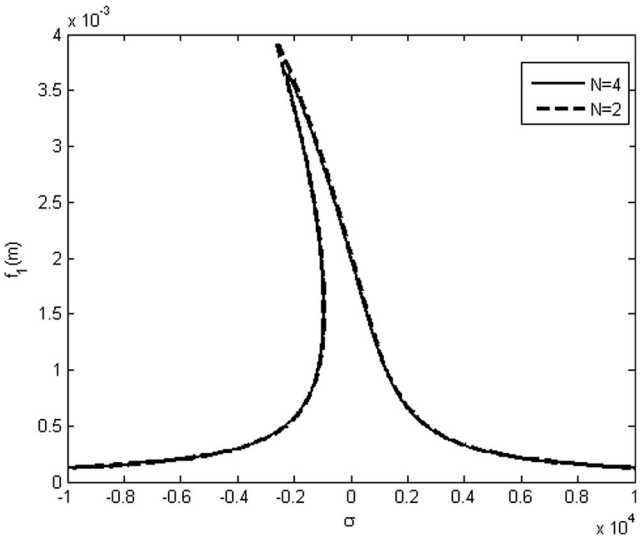

Fig. 9 The effect of the number of cutter teeth on the frequency response of the tool tip vibration for the primary resonance case ($\Omega = \omega_1$)

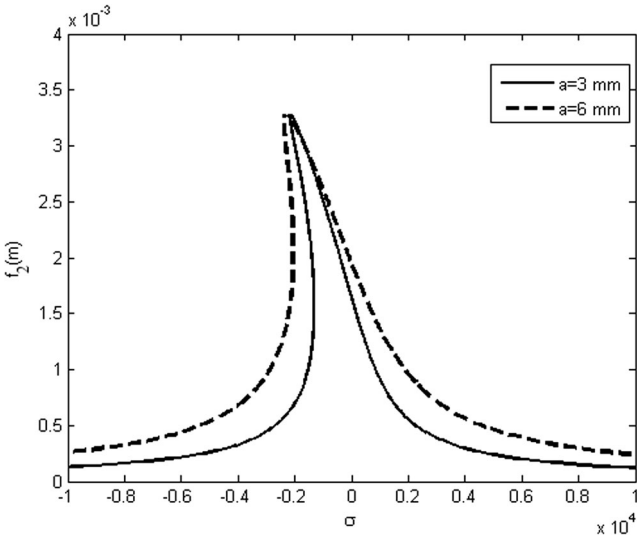

Fig. 10 The effect of axial depth of cut on the frequency response of the tool tip vibration for the primary resonance case ($\Omega = \omega_2$)

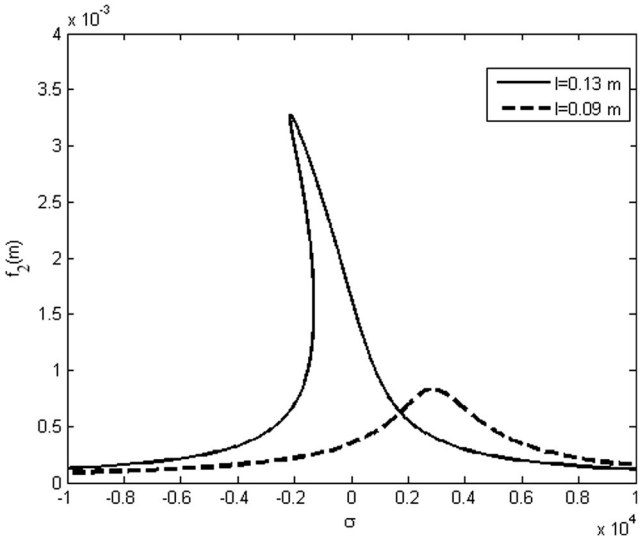

Fig. 12 The effect of cutting tool length on the frequency response of the tool tip vibration for the primary resonance case ($\Omega = \omega_2$)

3. Steps 1 and 2 have been repeated for other tool rotational speeds.
4. Stability diagram has been plotted between different points obtained in step 2.

Constructed stability diagram for the milling process is presented in Fig. 4. Also this figure shows the stability diagram when gyroscopic moment and rotary inertia have not been considered. It can be seen from Fig. 4 that the results predicted by the current model with considering gyroscopic moment and rotary inertia are in reasonable agreement with the experimental results. Also according to this figure, ignoring gyroscopic moment and rotary inertia in the tool model causes error in the prediction of stability limits of the process.

6.2 Primary resonance

To investigate the nonlinear dynamics of the milling process, a realistic nominal set of the process parameters is adopted for simulation as presented in Table 1.

For the case of primary resonance ($\Omega = \omega_1$), according to Eq. (50), the frequency response of the tool tip vibration is presented in Fig. 5. As it is observed, increasing the detuning parameter from point A to point C leads to a gradual increase in steady state vibration amplitude. At

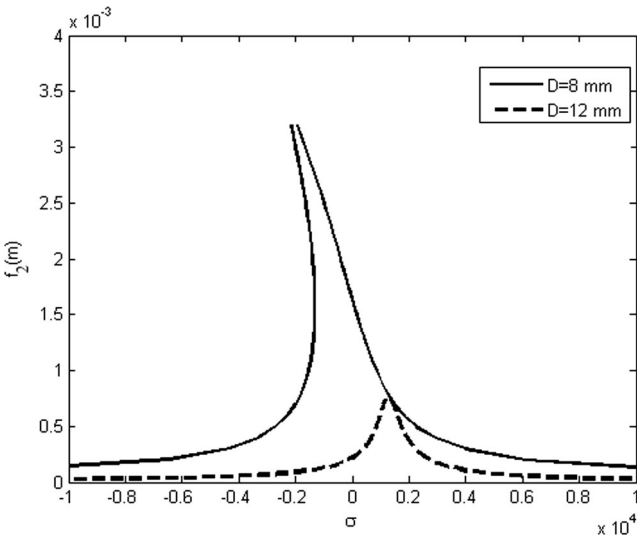

Fig. 11 The effect of cutting tool diameter on the frequency response of the tool tip vibration for the primary resonance case ($\Omega = \omega_2$)

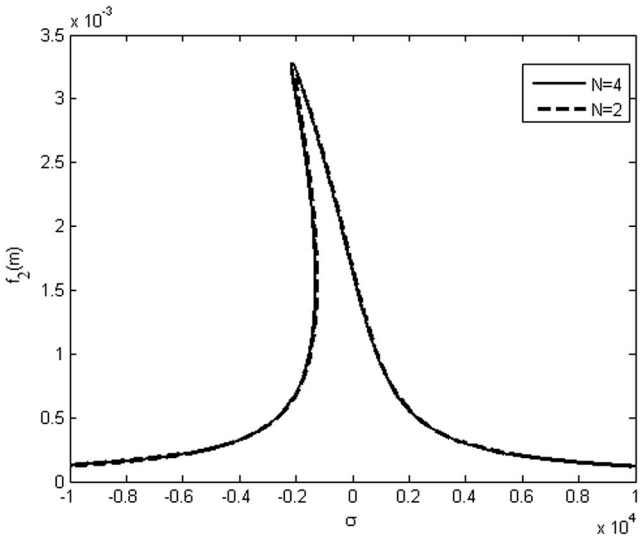

Fig. 13 The effect of the number of cutter teeth on the frequency response of the tool tip vibration for the primary resonance case ($\Omega = \omega_2$)

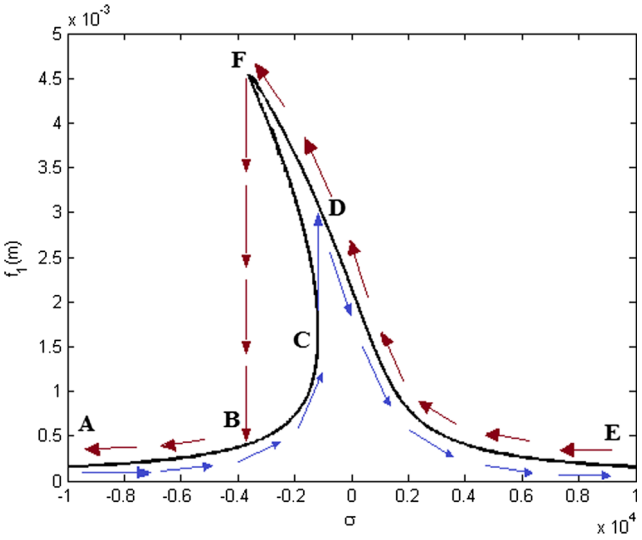

Fig. 14 Frequency response of the tool tip vibration for the super harmonic resonance case ($2\Omega = \omega_1$)

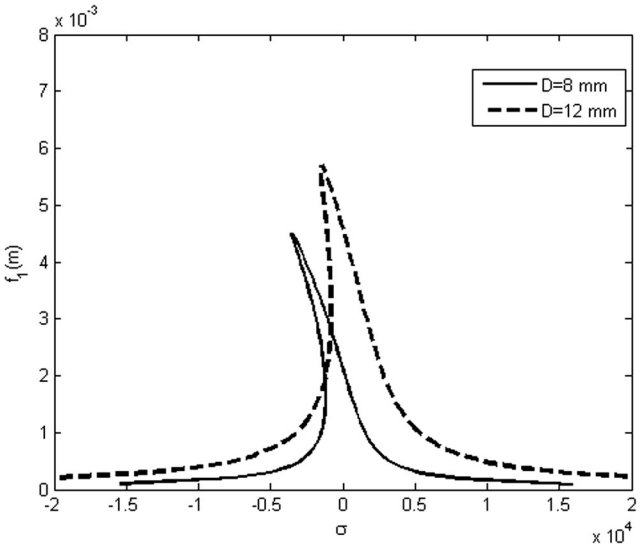

Fig. 16 The effect of cutting tool diameter on the frequency response of the tool tip vibration for the super harmonic resonance case ($2\Omega = \omega_1$)

point C, upward jump occurs to point D. After that, by increasing the detuning parameter, vibration amplitude decreases. On the other hand, as σ is decreased from point E to F, steady state vibration amplitude increases; and at point F, there is a downward jump to the point B.

Figures 6, 7, 8, and 9 show effects of axial depth of cut, cutting tool diameter, cutting tool length, and the number of cutter teeth on the frequency response of the tool tip vibrations, respectively. As it is shown in Figs. 6 and 8, by increasing the axial depth of cut and cutting tool length, steady state amplitude of vibration of the tool tip increase. Also in accordance with Fig. 7, increase in cutting tool diameter decreases the steady state amplitude of vibration of the tool tip. As shown in Fig. 9, variation of the cutter teeth number has small effect on frequency response of the system.

The effects of axial depth of cut, cutting tool diameter, cutting tool length, and the number of cutter teeth on the frequency response of the tool tip vibrations for another primary resonance case ($\Omega = \omega_2$) are presented in Figs. 10, 11, 12, and 13. As shown in these figures, the results are similar to frequency response of primary resonance ($\Omega = \omega_1$).

6.3 Super harmonic resonance

Frequency response of the tool tip vibration for the super harmonic resonance case ($2\Omega = \omega_1$) in accordance with Eq. 56 is presented in Fig. 14. According to this figure, if the detuning parameter is started at point E and is slowly decreased, a jump from point F to point B takes place. On

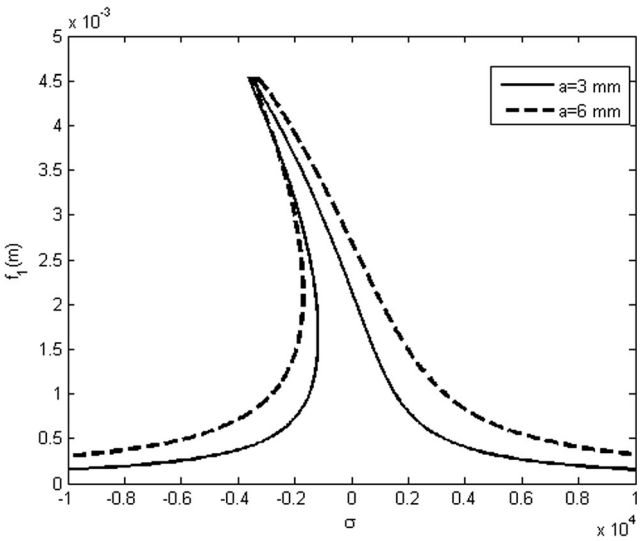

Fig. 15 The effect of axial depth of cut on the frequency response of the tool tip vibration for the super harmonic resonance case ($2\Omega = \omega_1$)

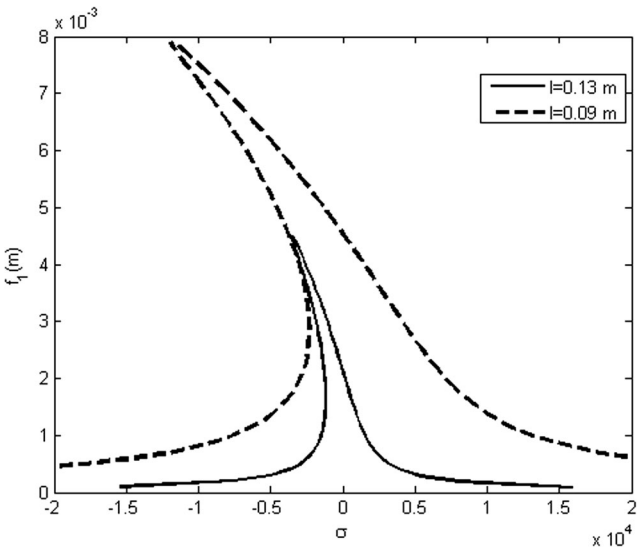

Fig. 17 The effect of cutting tool length on the frequency response of the tool tip vibration for the super harmonic resonance case ($2\Omega = \omega_1$)

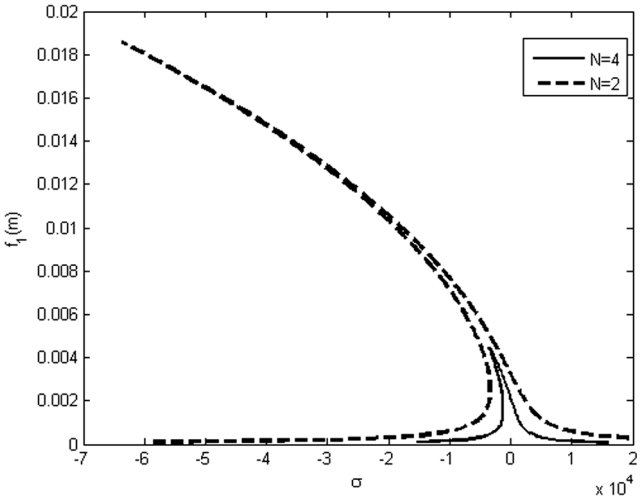

Fig. 18 The effect of the number of cutter teeth on the frequency response of the tool tip vibration for the super harmonic resonance case ($2\Omega = \omega_1$)

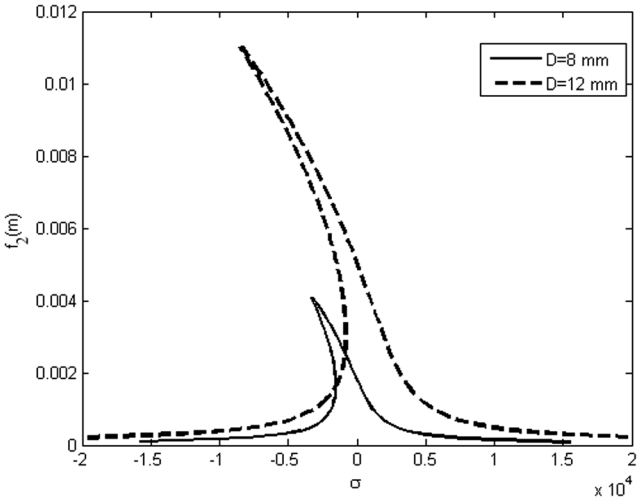

Fig. 20 The effect of cutting tool diameter on the frequency response of the tool tip vibration for the super harmonic resonance case ($2\Omega = \omega_2$)

the other hand, if the detuning parameter is started at point A and is increased, a jump from point C to point D takes place.

The effects of axial depth of cut, cutting tool diameter and length, and the number of cutter teeth on the frequency response of the tool tip vibrations for this case ($2\Omega = \omega_1$) are shown in Figs. 15, 16, 17, and 18. Effect of axial depth of cut on frequency response function for this case is similar to primary resonance cases. According to Fig. 16, with increase in cutting tool diameter, the steady state amplitude of the tool tip vibration increases and the curvature of the back bone curve decreases. Also as shown in Figs. 17 and 18 with increase in the cutting tool length and cutter teeth number, the steady state amplitude of the tool tip vibration decreases.

Figures 19, 20, 21, and 22 show the effects of different parameters on the frequency response of the tool tip vibrations for super harmonic case ($2\Omega = \omega_2$). As shown in these figures, effects of axial depth of cut, cutting tool diameter and length, and the number of cutter teeth on frequency response function for this case are similar to super harmonic case ($2\Omega = \omega_1$).

To investigate the effect of the gyroscopic moment and rotary inertia on the response of the system, frequency responses of the tool tip vibration with and without considering gyroscopic moment and rotary inertia are presented in Figs. 23, 24, 25, and 26 for different primary and super harmonic resonances. According to these figures, ignoring gyroscopic moment and rotary inertia in the tool model decreases the predicted amplitude of steady state response of the system.

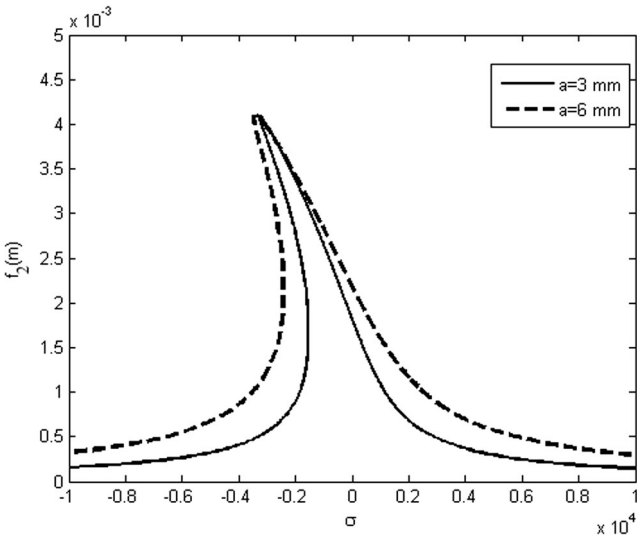

Fig. 19 The effect of axial depth of cut on the frequency response of the tool tip vibration for the super harmonic resonance case ($2\Omega = \omega_2$)

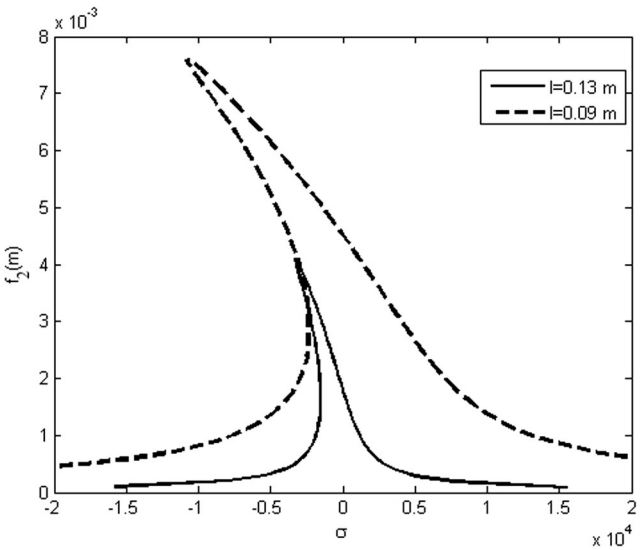

Fig. 21 The effect of cutting tool length on the frequency response of the tool tip vibration for the super harmonic resonance case ($2\Omega = \omega_2$)

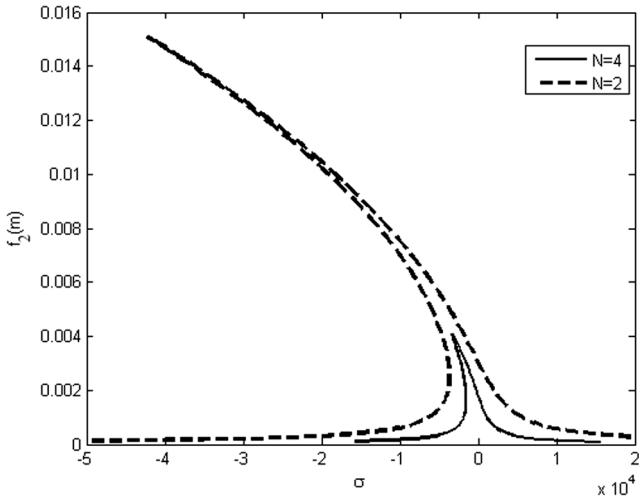

Fig. 22 The effect of the number of cutter teeth on the frequency response of the tool tip vibration for the super harmonic resonance case ($2\Omega = \omega_2$)

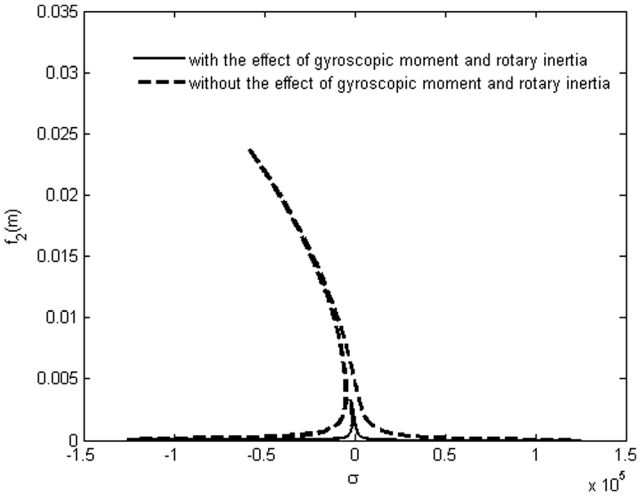

Fig. 24 The effect of the gyroscopic moment and rotary inertia on the frequency response of the tool tip vibration for the primary resonance case ($\Omega = \omega_2$)

7 Conclusion

In this paper, resonance in milling process has been investigated using a 3-D nonlinear model of the cutting tool. The tool has been modeled as a rotating clamped-free beam excited by nonlinear cutting forces. The complete system equations have been obtained for vertical and lateral beam vibrations. This model considers gyroscopic moment and rotary inertia of the tool. The method of multiple scales has been used to obtain the analytical expression for frequency response of the system.

Using this model, primary and super harmonic resonances of cutting tool have been investigated and following results have been obtained:

1- Increase of axial depth of cut increases the steady state vibration amplitude of the tool tip in all resonance case.
2- With increase in cutting tool diameter, the steady state vibration response of the tool tip decreases for primary resonance cases and increases for super harmonic resonance cases.
3- With increase in cutting tool length, the steady state vibration response of the tool tip increases for primary resonance cases and decreases for super harmonic resonance cases.
4- Variation of the number of cutter teeth has negligible effect on the frequency response of the system in primary resonances, but it extremely changes the steady state vibration response of the tool tip in super harmonic resonances.

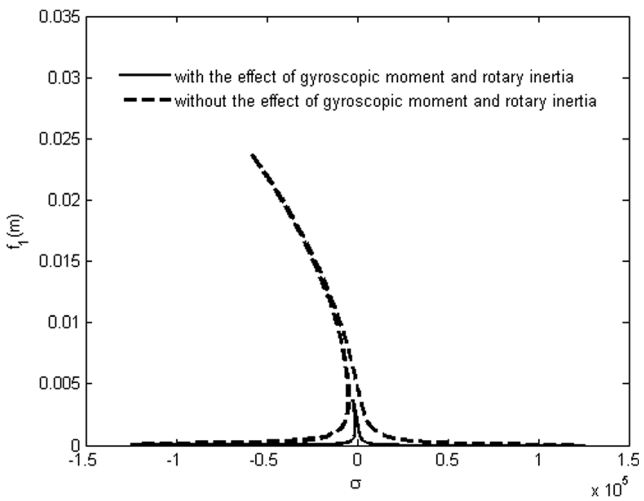

Fig. 23 The effect of the gyroscopic moment and rotary inertia on the frequency response of the tool tip vibration for the primary resonance case ($\Omega = \omega_1$)

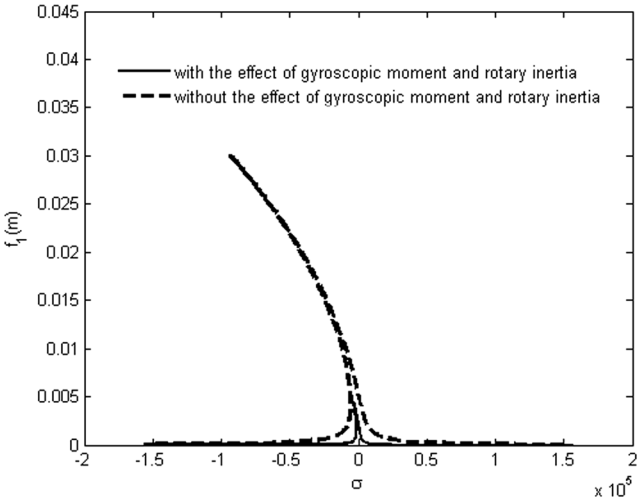

Fig. 25 The effect of the gyroscopic moment and rotary inertia on the frequency response of the tool tip vibration for the super harmonic resonance case ($2\Omega = \omega_1$)

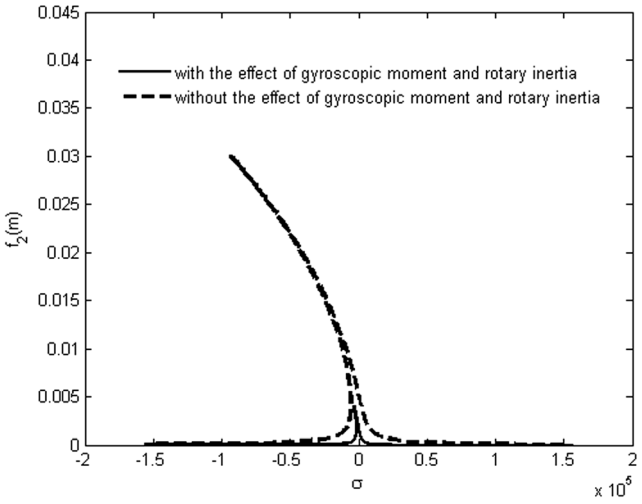

Fig. 26 The effect of the gyroscopic moment and rotary inertia on the frequency response of the tool tip vibration for the super harmonic resonance case ($2\Omega = \omega_2$)

Appendix A

$$A_{1i} = \int_0^l \left(EIV_i(x)^{\prime\prime\prime\prime}\right)\mathrm{V_i}(x)dx$$

$$A_{2i} = -\int_0^l 1.5EAv_{i(x)}^{\prime 2} v_{i(x)}^{\prime\prime} v_{i(x)} dx$$

$$A_{3i} = -\int_0^l \left[0.5EAv_{i(x)}^{\prime\prime} w_{i(x)}^{\prime 2} v_{i(x)} - EAv_{i(x)}^{\prime} w_{i(x)}^{\prime} w_{i(x)}^{\prime\prime} v_{i(x)}\right] dx$$

$$A_{4i} = \int_0^l \left(-2\rho IW_i(x)^{\prime\prime}\right)\mathrm{V_i}(x)dx$$

$$A_{5i} = \int_0^l \left(mV_i(x) - \rho IV_i(x)^{\prime\prime}\right)\mathrm{V_i}(x)dx$$

$$A_{6i} = -\frac{N}{2\pi}\alpha_0 \int_0^l (\mathrm{V_i(x)}\delta_\mathrm{D}(\mathrm{x}-\mathrm{x_0}))\mathrm{V_i}(x)dx$$

$$A_{7i} = -\frac{N}{2\pi}\beta_0 \int_0^l (\mathrm{W_i(x)}\delta_\mathrm{D}(\mathrm{x}-\mathrm{x_0}))\mathrm{V_i}(x)dx$$

$$A_{8i} = \left(-\frac{N}{2\pi}\gamma_0 - \frac{c_f}{2}\eta_1\right)\int_0^l (\delta_\mathrm{D}(\mathrm{x}-\mathrm{x_0}))\mathrm{V_i}(x)dx$$

$$A_{9i} = \int_0^l (\delta_\mathrm{D}(\mathrm{x}-\mathrm{x_0}))\mathrm{V_i}(x)dx$$

$$B_{1i} = \int_0^l \left(EIW_i(x)^{\prime\prime\prime\prime}\right)\mathrm{W_i}(x)dx$$

$$B_{2i} = -\int_0^l 1.5EAw_{i(x)}^{\prime 2} w_{i(x)}^{\prime\prime} w_{i(x)} dx$$

$$B_{3i} = -\int_0^l \left[0.5EAw_{i(x)}^{\prime\prime} v_{i(x)}^{\prime 2} w_{i(x)} + EAv_{i(x)}^{\prime} w_{i(x)}^{\prime} v_{i(x)}^{\prime\prime} w_{i(x)}\right] dx$$

$$B_{4i} = \int_0^l (2\rho IV_i(\mathrm{x})^{\prime\prime})\mathrm{W_i}(x)dx$$

$$B_{5i} = \int_0^l \left(mW_i(x) - \rho IW_i(x)^{\prime\prime}\right)\mathrm{W_i}(x)dx$$

$$B_{6i} = \frac{N}{2\pi}\alpha^{\prime}{}_0 \int_0^l (\mathrm{V_i(x)}\delta_\mathrm{D}(\mathrm{x}-\mathrm{x_0}))\mathrm{W_i}(x)dx$$

$$B_{7i} = \frac{N}{2\pi}\beta^{\prime}{}_0 \int_0^l (\mathrm{W_i(x)}\delta_\mathrm{D}(\mathrm{x}-\mathrm{x_0}))\mathrm{W_i}(x)dx$$

$$B_{8i} = \left(\frac{N}{2\pi}\gamma^{\prime}{}_0 + \frac{c_f}{2}\zeta_1\right)\int_0^l (\delta_\mathrm{D}(\mathrm{x}-\mathrm{x_0}))\mathrm{W_i}(x)dx$$

$$B_{9i} = \int_0^l (\delta_\mathrm{D}(\mathrm{x}-\mathrm{x_0}))\mathrm{W_i}(x)dx$$

Appendix B

$$P_1 = \left(\frac{1}{-(2i\Omega)^4 A_{4i}^{\prime} + \left(-A_{1i}^{\prime} - B_{1i}^{\prime} + B_{4i}^{\prime}A_{4i}^{\prime}\right)(2i\Omega)^2 - A_{1i}^{\prime}B_{1i}^{\prime}}\right)\left(\frac{c_f}{2}\left(A_{9i}^{\prime}(2i\Omega)^2\zeta_1 + A_{9i}^{\prime}B_{1i}^{\prime}\zeta_1 + A_{4i}^{\prime}B_{9i}^{\prime}2\Omega\zeta_1\right)\right)$$

$$P_2 = \left(\frac{1}{-(2i\Omega)^4 A'_{4i} + \left(-A'_{1i} - B'_{1i} + B'_{4i}A'_{4i}\right)(2i\Omega)^2 - A'_{1i}B'_{1i}}\right)\left(-\frac{c_f}{2}\left(A'_{9i}(2i\Omega)^2\eta_1 + A'_{9i}B'_{1i}\eta_1 + A'_{4i}B'_{9i}2\Omega\eta_1\right)\right)$$

$$P_3 = \left(\frac{1}{-(i\Omega)^4 A'_{4i} + \left(-A'_{1i} - B'_{1i} + B'_{4i}A'_{4i}\right)(i\Omega)^2 - A'_{1i}B'_{1i}}\right)\left(A'_{9i}(i\Omega)^2\eta_2 + A'_{9i}B'_{1i}\eta_2 + A'_{4i}B'_{9i}\Omega\eta_2\right)$$

$$P_4 = \left(\frac{1}{-(i\Omega)^4 A'_{4i} + \left(-A'_{1i} - B'_{1i} + B'_{4i}A'_{4i}\right)(i\Omega)^2 - A'_{1i}B'_{1i}}\right)\left(A'_{9i}(i\Omega)^2\zeta_2 + A'_{9i}B'_{1i}\zeta_2 + A'_{4i}B'_{9i}\Omega\zeta_2\right)$$

$$P_5 = \left(\frac{1}{-(2\Omega)^2 + B'_{1i}}\right)\left(-\frac{c_f}{2}B'_{9i}\eta_1 + P_2B'_{4i}(2\Omega)\right)$$

$$P_6 = \left(\frac{1}{-(2\Omega)^2 + B'_{1i}}\right)\left(-\frac{c_f}{2}B'_{9i}\xi_1 - P_1B'_{4i}(2\Omega)\right)$$

$$P_7 = \left(\frac{1}{-(\Omega)^2 + B'_{1i}}\right)\left(B'_{9i}\xi_2 + P_4B'_{4i}\Omega\right)$$

$$P_8 = \left(\frac{1}{-(\Omega)^2 + B'_{1i}}\right)\left(-B'_{9i}\eta_2 - P_3B'_{4i}\Omega\right)$$

Appendix C

$$\lambda_{1r} = 0$$

$$\lambda_{1i} = -i\left(-2i\omega_1 - A'_{4i}\Lambda_1 - 2i\omega_1\Lambda_1\overline{\Lambda}_1 - B'_{4i}\overline{\Lambda}_1\right)$$

$$\lambda_{2r} = \left(A'_{6i}(1-\cos(\omega_1\tau)) + A'_{7i}i\Lambda_1\sin(\omega_1\tau) + B'_{6i}i\overline{\Lambda}_1\sin(\omega_1\tau) + B'_{7i}\Lambda_1\overline{\Lambda}_1(1-\cos(\omega_1\tau))\right)$$

$$\lambda_{2i} = -i\left(A'_{6i}i\sin(\omega_1\tau)\right) + A'_{7i}\Lambda_1(1-\cos(\omega_1\tau)) + B'_{6i}\overline{\Lambda}_1(1-\cos(\omega_1\tau)) + B'_{7i}i\Lambda_1\overline{\Lambda}_1\sin(\omega_1\tau)\Big)$$

$$\lambda_{3r} = -6A'_{2i} - 3A'_{3i}\Lambda_2\overline{\Lambda}_2 - 2A'_{3i}\Lambda_1\overline{\Lambda}_2 - 2A'_{3i}\Lambda_1\Lambda_2 - 6B'_{2i}\Lambda_1\overline{\Lambda}_1\Lambda_2\overline{\Lambda}_2 - 2B'_{3i}\Lambda_1\overline{\Lambda}_1 - 2B'_{3i}\overline{\Lambda}_1\Lambda_2 - 2B'_{3i}\overline{\Lambda}_1\overline{\Lambda}_2$$

$$\lambda_{3i} = 0$$

$$\lambda_{4r} = -3A'_{2i} - A'_{3i}{\Lambda_1}^2 - 2A'_{3i}\Lambda_1\overline{\Lambda}_1 - 3B'_{2i}{\Lambda_1}^2{\overline{\Lambda}_1}^2 - B'_{3i}{\overline{\Lambda}_1}^2 - 2B'_{3i}\Lambda_1\overline{\Lambda}_1$$

$$\lambda_{4i} = 0$$

$$\lambda_{5r} = 0$$

$$\lambda_{5i} = -i\left(-2i\omega_2 - A'_{4i}\Lambda_2 - 2i\omega_2\Lambda_2\overline{\Lambda}_2 - B'_{4i}\overline{\Lambda}_2\right)$$

$$\lambda_{6r} = \left(A'_{6i}(1-\cos(\omega_2\tau)) + A'_{7i}i\Lambda_2\sin(\omega_2\tau) + B'_{6i}i\overline{\Lambda}_2\sin(\omega_2\tau) + B'_{7i}\Lambda_2\overline{\Lambda}_2(1-\cos(\omega_2\tau))\right)$$

$$\lambda_{6i} = -i\left(A'_{6i}i\sin(\omega_2\tau)\right) + A'_{7i}\Lambda_2(1-\cos(\omega_2\tau)) + B'_{6i}\overline{\Lambda}_2(1-\cos(\omega_2\tau)) + B'_{7i}i\Lambda_2\overline{\Lambda}_2\sin(\omega_2\tau)\Big)$$

$$\lambda_{7r} = -6A'_{2i} - 3A'_{3i}\Lambda_1\overline{\Lambda}_1 - 2A'_{3i}\Lambda_2\overline{\Lambda}_1 - 2A'_{3i}\Lambda_1\Lambda_2 - 6B'_{2i}\Lambda_1\overline{\Lambda}_1\Lambda_2\overline{\Lambda}_2 - 2B'_{3i}\Lambda_2\overline{\Lambda}_2 - 2B'_{3i}\overline{\Lambda}_2\Lambda_1 - 2B'_{3i}\overline{\Lambda}_1\overline{\Lambda}_2$$

$$\lambda_{7i} = 0$$

$$\lambda_{8r} = -3A'_{2i} - A'_{3i}{\Lambda_2}^2 - 2A'_{3i}\Lambda_2\overline{\Lambda}_2 - 3B'_{2i}{\Lambda_2}^2{\overline{\Lambda}_2}^2 - B'_{3i}{\overline{\Lambda}_2}^2 - 2B'_{3i}\Lambda_2\overline{\Lambda}_2$$

$$\lambda_{8i} = 0$$

References

1. Balachandran B, Zhao MX (2000) A mechanics based model for study of dynamics of milling operations. Meccanica 35:89–109
2. Mann BP, Garg NK, Young KA, Helvey AM (2005) Milling bifurcations from structural asymmetry and nonlinear regeneration. Nonlinear Dyn 42:319–337
3. Vela-Martinez L, Jauregui-Correa JC, Gonzalez-Brambila OM, Herrera-Ruiz G, Lozano-Guzman A (2009) Instability conditions due to structural nonlinearities in regenerative chatter. Nonlinear Dyn 56(4):415–427
4. Altintas Y, Budak E (1995) Analytical prediction of stability lobes in milling. CIRP Ann 44(1):357–362
5. Banihasan M, Bakhtiari-Nejad F (2011) Chaotic vibrations in high-speed milling. Nonlinear Dyn 66:557–574
6. Moradi H, Vossoughi G, Movahhedy MR (2014) Bifurcation analysis of nonlinear milling process with tool wear and process damping: sub-harmonic resonance under regenerative chatter. Int J Mech Sci 85:1–19
7. Campa FJ, Lopez de Lacalle LN, Celaya A (2011) Chatter avoidance in the milling of thin floors with bull-nose end mills: model and stability diagrams. Int J Mach Tool Manu 51:43–53
8. Compean FI, Olvera D, Campa FJ, Lopez de Lacalle LN, Elias A, Rodriguez CA (2012) Stability prediction in straight turning of a flexible workpiece by collocation method. Int J Mach Tool Manu 57:27–33
9. Peng C, Wang L, Liao TW (2015) A new method for the prediction of chatter stability lobes based on dynamic cutting force simulation model and support vector machine. J Sound Vib 345:118–131
10. Wan M, Ma YC, Feng J, Zhang WH (2016) Study of static and dynamic ploughing mechanisms by establishing generalized model with static milling forces. Int J Mech Sci 114:120–131
11. Wan M, Kilic ZM, Altintas Y (2015) Mechanics and dynamics of multifunctional tools. J Manuf Sci E-T ASME 137:1–11
12. Wan M, Ma YC, Zhang WH, Yang Y (2015) Study on the construction mechanism of stability lobes in milling process with multiple modes. Int J Adv Manuf Tech 79:589–603
13. Wan M, Altintas Y (2014) Mechanics and dynamics of thread milling process. Int J Mach Tool Manu 87:16–26
14. Wang M, Gao L, Zheng Y (2014) Prediction of regenerative chatter in the high-speed vertical milling of thin-walled workpiece made of titanium alloy. Int J Adv Manuf Tech 72:707–716
15. Yang Y, Liu Q, Zhang B (2014) Three-dimensional chatter stability prediction of milling based on the linear and exponential cutting force model. Int J Adv Manuf Tech 72:1175–1185
16. Qu S, Zhao J, Wang T (2016) Three-dimensional stability prediction and chatter analysis in milling of thin-walled plate. Int J Adv Manuf Tech 86:2291–2300
17. Liu Y, Meng LL, Liu K, Zhang YM (2016) Chatter reliability of milling system based on first-order second-moment method. Int J Adv Manuf Tech. doi:10.1007/s00170-016-8523-6
18. Yue C, Liu X, Liang SY (2016) A model for predicting chatter stability considering contact characteristic between milling cutter and workpiece. Int J Adv Manuf Tech. doi:10.1007/s00170-016-8953-1
19. Liu B, Zhu L, Dun Y, Liu C (2016) Investigation on chatter stability of thin-walled parts in milling based on process damping with relative transfer functions. Int J Adv Manuf Tech. doi:10.1007/s00170-016-9431-5
20. Moradi H, Movahhedy MR, Vossoughi G (2012) Bifurcation analysis of milling process with tool wear and process damping: regenerative chatter with primary resonance. Nonlinear Dyn 70(1):481–509
21. Moradi H, Vossoughi G, Movahhedy MR, Ahmadian MT (2013) Forced vibration analysis of the milling process with structural nonlinearity, internal resonance, tool wear and process damping effects. Int J Nonlinear Mech 54:22–34
22. Moradi H, Movahhedy MR, Vossoughi G (2012) Dynamics of regenerative chatter and internal resonance in milling process with structural and cutting force nonlinearities. J Sound Vib 331:3844–3865
23. Nakano Y, Takahara H, Yasue K, Asaga R (2012) The effect of multiple dynamic absorbers on regenerative chatter and resonance in end milling process. Proceedings of the ASME 2012 International Mechanical Engineering Congress & Exposition, IMECE2012–87218, November 9–15, 2012, Houston, Texas, USA
24. Nayfeh AH, Pai PF (2004) Linear and nonlinear structural mechanics. Wiley Interscience, New York
25. Hosseini SAA, Khadem SE (2009) Free vibrations analysis of a rotating shaft with nonlinearities in curvature and inertia. Mech Mach Theory 44:272–288
26. Meirovitch L (1997) Principles and techniques of vibrations. Prentice-Hall, New Jersey
27. Altintas Y (2000) Manufacturing automation: metal cutting mechanics, machine tool vibrations, and CNC design. Cambridge University Press
28. Ishida Y, Yamamoto T (2012) Linear and nonlinear rotor dynamics: a modern treatment with applications. Wiley, New York
29. Hodges DH, Dowell EH (1974) Nonlinear equations of motion for the elastic bending and torsion of twisted nonuniform rotor blades. NASA technical note
30. Nayfeh AH, Mook D (1979) Nonlinear oscillations. Wiley, New York
31. Moradi H, Vossoughi G, Movahhedy MR (2013) Experimental dynamic modelling of peripheral milling with process damping, structural and cutting force nonlinearities. J Sound Vib 332:4709–4731